Dalton Transactions

ROYAL SOCIETY OF CHEMISTRY

PAPER

View Article Online
View Journal | View Issue

Cite this: *Dalton Trans.*, 2026, **55**, 2071

Pr-doped NiFe-layered double hydroxide on plasma-etched nickel foam as a high-efficiency electrocatalyst for oxygen evolution reaction

Jian-Long Lei, Shui-Sheng Li, Xi Zhen, Lu Shen and Bin He *

Received 6th November 2025,
Accepted 7th January 2026

DOI: 10.1039/d5dt02658j

rsc.li/dalton

Nickel-iron layered double hydroxide (NiFe-LDH), as a highly promising non-precious metal catalyst for the oxygen evolution reaction (OER), still suffers from several inherent drawbacks, including poor electrical conductivity, insufficient exposure of active sites, and a decline in performance under high current densities. These limitations severely restrict its practical application in the oxygen evolution reaction. Herein, a nanosheet morphology Pr-doped NiFe layered double hydroxide catalysts (Pr-NiFe-LDH) was synthesized *in situ* on the surface of Nickel foam modified by dielectric barrier discharge (DBD) plasma (PNF). The addition of Pr elements can effectively adjust the electronic structure of NiFe-LDH, change the position of the d-band center, and increase the number of active sites, thereby enhancing the catalytic activity. The overpotential of Pr-NiFe-LDH was reduced to 321 mV at 100 mA cm^{-2}, significantly lower than that of NiFe-LDH (342 mV) and even superior to that of commercial RuO_2 catalyst (441 mV). The density functional theory (DFT) study indicates that adding Pr to the surface of NiFe-LDH enhances its performance in the OER. This work not only deepened the understanding of the OER mechanism in the NiFe-LDH catalyst, but also provided valuable insights for the design of efficient, low-cost and noble-metal-free electrocatalysts.

1. Introduction

The oxygen evolution reaction (OER) is a critical process in renewable energy technologies such as water splitting, CO_2 reduction and metal–air batteries as it directly affects the overall efficiency of these systems.[1–3] The efficiency of the OER plays a decisive role in the energy conversion and storage performance of these applications. However, its practical efficiency is severely hindered by sluggish reaction kinetics and the high overpotential required to achieve desirable reaction rates. These challenges pose significant obstacles to the widespread adoption of OER in technologies like water splitting and fuel cells. At present, noble metal catalysts such as RuO_2 and IrO_2 are the benchmark materials for the OER due to their exceptional catalytic properties.[4,5] These catalysts enable efficient oxygen evolution at relatively low overpotentials and exhibit outstanding catalytic activity. Nevertheless, they face issues such as limited availability and high cost, which present major economic challenges for large-scale applications. Moreover, although these noble metal catalysts demonstrate certain stability, they are prone to degradation or deactivation under high current density conditions. Therefore, it is highly necessary to design and investigate earth-abundant, cost-effective, non-precious metal-based electrocatalysts for the oxygen evolution reaction.

Currently, layered double hydroxides (LDHs) have attracted increasing attention due to their unique morphology, adjustable interlayer structure, doping elements, excellent OER catalytic performance, and simple synthesis methods. The oxygen evolution reaction (OER) activity of LDHs still needs to be further enhanced through additional processing methods in order to achieve a higher current density.[6,7] A feasible strategy is to optimize the structure and composition of LDHs. From the perspective of structural optimization, combining LDHs with a foam substrate can improve conductivity, thereby enhancing the OER catalytic performance. The growth of materials on a foam substrate has the following advantages: 1. The Nickel foam providing an efficient electron transmission channel for the active materials, significantly reducing the internal resistance of the electrode, and being particularly beneficial for reactions under high current density. 2. Through *in situ* growth technology, the active material is firmly bonded to the substrate, eliminating the need for traditional adhesives. This significantly enhances the structural stability and cycle life of the electrode, preventing the detachment of

Zhejiang Key Laboratory for Industrial Solid Waste Thermal Hydrolysis Technology and Intelligent Equipment, Huzhou Key Laboratory of Environmental Functional Materials and Pollution Control, Department of Materials Engineering, Huzhou University, Huzhou 313000, China. E-mail: binhe@zjhu.edu.cn

active substances. 3. Its high porosity and large specific surface area provide a vast space for loading active materials, exposing more active sites, and facilitating electrolyte infiltration, ion transmission, and reaction gas escape.[8,9] Recently, an increasing number of studies have shown that the doping of heteroatoms (transition metal elements and non-metal elements, *etc.*) can alter the valence of elements and adjust the electronic structure of layered double hydroxides (LDHs), thereby ultimately influencing their catalytic activity.[10–13] In other words, choosing the appropriate doped elements is crucial for enhancing the catalytic activity of LDHs. Rare earth elements have driven the development of industrial technology. Their unique 4f electronic structure and multiple variable valence states endow them with unique catalytic properties. From the perspective of component optimization, incorporating a small amount of rare earth elements into layered double hydroxides (LDHs) can significantly improve the performance of the oxygen evolution reaction (OER). For example, Li *et al.* proposed that in the cerium-doped nickel-iron layered hydroxide, there exists a lattice distortion. This distortion enhances the performance of the oxygen evolution reaction (OER) by increasing the available surface area and promoting the formation of more oxygen vacancies, thereby optimizing the adsorption energy of the intermediate species and altering the electronic structure.[14] We utilized the stronger electronegativity of rare earth yttrium ions (Y^{3+}) to *in situ* induce NiCo layered double hydroxide nanosheets (NCF) from NiCo foam (NCF) treated by dielectric barrier discharge plasma. Then, after phosphating treatment in nitrogen gas using radio frequency plasma, nitrogen-doped YNiCo phosphide (N-YNiCoP/PNCF) was obtained. The coordination number of CoNi decreased with the incorporation of Y atoms, which led to shorter bonds between Ni and Co ions, facilitating the open educational resources of N-YNiCoP in HER and simulated industrial conditions.[15] Compared to pure NiCoP, the Pr-doped NiCoP exhibits significantly enhanced catalytic performance and stability. This work reveals that incorporating Pr ions introduces additional active sites for the hydrogen evolution reaction (HER), leading to improved overall catalytic activity.[16] These findings suggest that doping rare-earth elements into the lattice can effectively modulate both the electronic and crystal structures of the electrocatalyst, thereby boosting its catalytic efficiency. Despite these advances, the specific role of Praseodymium (Pr) in NiFe-LDHs remains less explored and warrants in-depth investigation. Pr, with its stable $Pr^{3+}/^{4+}$ mixed valence states, is anticipated to be a potent electronic modulator. We hypothesize that Pr doping can effectively perturb the d-band center of Ni/Fe sites, facilitate the formation of highly active Ni^{3+} species, and potentially participate in or promote favorable reaction pathways, leading to superior OER activity and stability.

Herein, we report a simple method of plasma etching and solvothermal method to fabrication of OER catalysts for water electrolysis. A Bubble-like shape Pr-doped NiFe layered double hydroxide catalysts (Pr-NiFe-LDH) was synthesized *in situ* on the surface of Nickel foam modified by dielectric barrier discharge (DBD) plasma (PNF), and the synthesized Pr-NiFe-LDH exhibits rich heterointerfaces and active sites, causing a high OER performance in an alkaline medium. The overpotential of Pr-NiFe-LDH was reduced to 321 mV at 100 mA cm^{-2}, significantly lower than that of NiFe-LDH (342 mV) and even superior to that of commercial RuO_2 catalyst (441 mV). Therefore, it stands out in the field of non-precious metal-based catalysts and becomes a highly competitive candidate. Its performance even surpasses the oxygen evolution electrocatalysts recently reported.

2. Experimental section

2.1 Chemicals and reagents

Ni foam (NF) (thickness: 0.1 cm) was purchased from Kunshan Xingzhenghong Electronic Materials Co., Ltd. The reagents, such as ethanol (CH_3CH_2OH), acetone (CH_3COCH_3), ferric nitrate nonahydrate ($Fe(NO_3)_3{\cdot}9H_2O$, 99.9%), urea (CH_4N_2O), ammonium fluoride (NH_4F), praseodymium nitrate hexahydrate ($Pr(NO_3)_3{\cdot}6H_2O$), nickel nitrate hexahydrate ($Ni(NO_3)_2{\cdot}6H_2O$) were purchased from the Aladdin Industrial Co., Ltd, China. In all experimental procedures, the deionized water was employed and all chemical reagents meet the standards of analytical grade.

2.2 PNF fabrication

Firstly, a piece of Ni foam (NF) was cut to a area of 2 × 2 cm^2, and then cleaned with acetone and a 1 M HCl solution 6 min in a 60 W ultrasonic bath. Afterwards, it was rinsed thoroughly with the anhydrous ethanol and deionized water for five cycles respectively, followed by drying in an oven at 50 °C for 10 min. Finally, both surfaces of the NF were treated for 10 minutes with an atmospheric pressure DBD plasma system.

2.3 Fabrication of Pr-NiFe-LDH/PNF

Synthesis of Pr-NiFe-LDH. Pr-NiFe-LDH grown on the PNF substrate was synthesized through a simple one-step hydrothermal process. To begin this synthesis, $Ni(NO_3)_2{\cdot}6H_2O$ (1.2 mmol), $Fe(NO_3)_3{\cdot}9H_2O$ (0.62 mmol), $Pr(NO_3)_3{\cdot}6H_2O$ (0.02 mmol), urea (6.8 mmol), and NH_4F (3.2 mmol) were first dissolved in 35 mL ultrapure water. Subsequently, the mixture was transported to a stainless-steel Teflon-lined autoclave, followed by a piece of PNF was immersed and heated to 120 °C for 12 hours. Finally, the sample was cleaned with water and dried at 60 °C. The preparation of NiFe LDH nanospheres only requires the removal of $Pr(NO_3)_3{\cdot}6H_2O$, with all other steps identical to those for NiFe-LDH.

2.4 Fabrication of RuO_2/PNF

2 mg of RuO_2 powder was dispersed into 1 mL mixture of ethanol containing 100 μL Nafion solution (5 wt%) by ultrasonication for 30 min. Then, RuO_2/NF electrodes were prepared by dropping the above solution onto the surface of NF.

2.5 Materials characterization

The morphological characteristics of the samples were examined using a scanning electron microscope (SEM, Hitachi S-4800) and a transmission electron microscope (TEM, JEM-2100F field emission TEM). Crystalline structures were identified *via* X-ray diffraction (XRD) on a Bruker D8 Advance diffractometer. Chemical states were probed by X-ray photoelectron spectroscopy (XPS) using an ESCALab MKII system.

2.6 Electrochemical measurements

The electrocatalytic performance of the catalysts was evaluated using a CHI 660E electrochemical workstation in a 1 M KOH electrolyte. Measurements were carried out using a standard three-electrode configuration, with the as-synthesized sample serving as the working electrode, a saturated calomel electrode (SCE) as the reference electrode, and a carbon rod as the counter electrode. All measured potentials were converted to the reversible hydrogen electrode (RHE) scale according to the Nernst equation:

$$E(\mathrm{RHE}) = E(\mathrm{SCE}) + 0.059 \times \mathrm{pH} + 0.241.$$

Linear sweep voltammetry (LSV) was performed at a scan rate of 5 mV s^{-1} with 85% iR compensation. Electrochemical impedance spectroscopy (EIS) was conducted in the frequency range from 10^5 Hz to 0.01 Hz with an AC amplitude of 10 mV. The long-term stability was evaluated by chronoamperometry (i–t) test at a constant potential that initially delivered ~20 mA cm^{-2} for 180 h.

2.7 Calculation methods and details

In this work, we use the Vienna *Abinitio* simulation package (VASP) for density flood theory (DFT + D3) calculations. The Perdew–Burke–Erzenhoff (PBE)[17] treatment of exchange–correlation interactions using the generalized gradient approximation (GGA)[18] function is employed. The projection-enhanced wave (PAW)[19] potential is used to characterize the interaction between valence electrons and nuclei. The energy cutoff is 450 eV. 2 × 2 × 1 gamma-centered k-point grid is used for Brillouin zone integration.[20] The energy convergence criterion was 1×10^{-5} eV. The internal coordinates of each system were fully optimized until the residual Hermann–Feynman force per atom was less than 0.05 eV $Å^{-1}$. The lattice length in the z-direction was set to be 18 Å to ensure that there was sufficient vacuum. The Gibbs free energy for each elemental step is calculated as $G = E_{elec} + E_{ZPE} - TS$, where E_{elec} is the electronic energy of the system, E_{ZPE} denotes the zero-point energy correction, and T is set to 298.15 K. VASPKIT[21] was used to post-process the computational results.

In the whole OER, the four-electron transfer process is expressed as the following four steps:

$$* + H_2O \rightarrow OH^* + H^+ + e^- \quad (1)$$

$$OH^* \rightarrow O^* + H^+ + e^- \quad (2)$$

$$O^* + H_2O \rightarrow OOH^* + H^+ + e^- \quad (3)$$

$$OOH^* \rightarrow O_2 + H^+ + e^- + * \quad (4)$$

* denotes the active site on the catalyst surface, O*, OH* and OOH* represent three intermediates involved in the entire four-electron process. The change in Gibbs free energy for every radical reaction was determined through the application of the subsequent equation:

$$\Delta G = \Delta E - T\Delta S + \Delta \mathrm{ZPE} \quad (5)$$

ΔZPE and ΔS are the variation in zero-point energy, derived from the vibrational frequency analysis of the adsorbate, compared to the entropy change at room temperature T (T = 298.15 K).[22]

The catalytic activity of OER was evaluated using the theoretical overpotential (η) in acidic solution, calculated as follows:

$$\eta^{\mathrm{OER}} = \max(\Delta G_1 + \Delta G_2 + \Delta G_3 + \Delta G_4)/e - 1.23 \quad (6)$$

3. Results and discussion

Pr-NiFe-LDH was fabricated by plasma-assisted treatment of foamed nickel combined with hydrothermal method. The entire synthesis process is shown in Fig. 1. In brief, the cleaned NF was first subjected to plasma treatment (DBD plasma) to obtain a rough surface, which resulted in abundant active sites and enhanced the binding strength between the plasma treatment Nickel foam (PNF) and the catalyst. Subsequently, a Pr-doped NiFe-LDH catalyst was synthesized by the hydrothermal method.

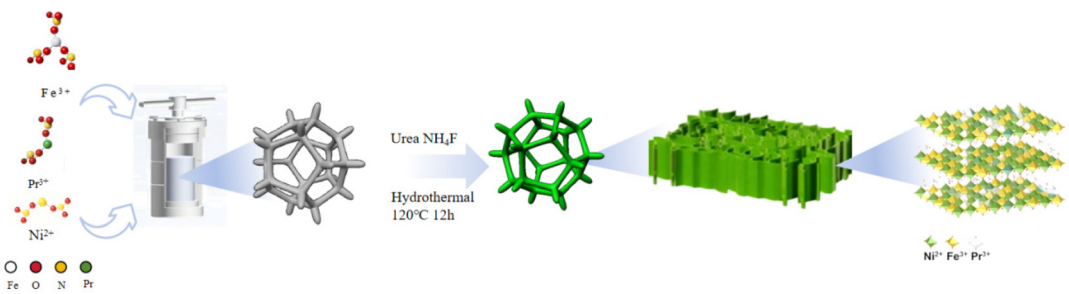

Fig. 1 Schematic illustration of the fabrication process of Pr-NiFe LDH on NF.

The XRD patterns of the as-prepared samples are presented in Fig. S1. The four characteristic diffraction peaks observed at 11.4°, 22.97°, 34.4°, and 38.99° can be assigned to the (003), (006), (012), and (015) crystal planes of NiFe-LDH (PDF #40-0215), respectively. Additionally, the diffraction peaks located at 44.5°, 51.8°, and 76.4° correspond to the (111), (200), and (220) planes of the Ni foam (NF) substrate (PDF #04-0850). Notably, the (003) diffraction peaks of the Pr-NiFe-LDH-are shifted compared to that of the undoped NiFe-LDH. This shift confirms the successful incorporation of Pr^{3+} ions into the NiFe-LDH structure without disrupting its layered architecture.[23]

The morphology and structure of the as-prepared catalysts were investigated using field-emission scanning electron microscopy (FE-SEM) and transmission electron microscopy (TEM). As seen in Fig. S2, this sample (Pr-NiFe-LDH) exhibits a nanosheet structure, and these nanosheets grow vertically on the nickel foam. Surprisingly, the thickness and size of the nanosheet structure observed at a scale of 500 nanometers are significantly thinner than those of NiFe-LDH, which effectively increased the exposed surface area. The construction of the thin sheet is expected to make more active sites visible, thereby facilitating the diffusion of substances and the transfer of charges. The nano-sheet morphology of Pr-NiFe LDH was further revealed through transmission electron microscopy (TEM) images (Fig. 2a and b), which were consistent with the aforementioned scanning electron microscopy (SEM) images.

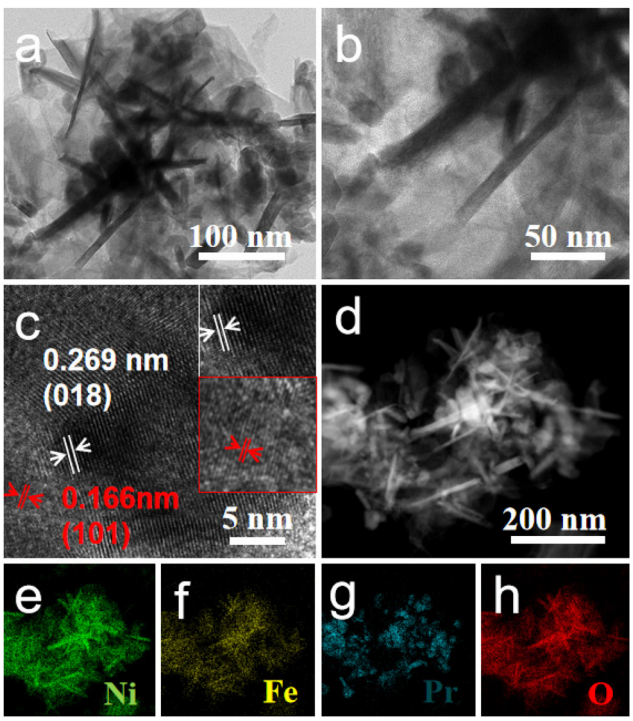

Fig. 2 (a and b) TEM and (c) HRTEM images of Pr-NiFe LDH, (d) HAADF-STEM image of Pr-NiFe LDH, (e–h) elemental mapping images of Pr-NiFe LDH.

Pr-NiFe LDH exhibited a three-dimensional nano-sheet structure that was vertically arranged and interconnected. The lattice stripe spacing of the twin structure are 0.166 and 0.269 nm, respectively, which can be associated with the (101) and (018) crystal faces of NiFe-LDH/NF, indicating lattice distortion due to Pr doping, which were in agreement with the XRD pattern (Fig. 2c). As evidenced by the EDS mapping in Fig. 2e–h, the elements Ni, Fe, Pr, and O are all uniformly distributed in the Pr-NiFe LDH, confirming the successful incorporation of Pr. Meanwhile, the nitrogen adsorption–desorption isotherms (Fig. S3a) of Pr-NiFe LDH exhibit typical Type-IV curves with H3-type hysteresis loops, confirming the presence of mesoporous structures. The structural advantages of the doped material are evidenced by its improved textural properties. It possesses a BET specific surface area of 55.9 $m^2\ g^{-1}$ and an average pore diameter of 15.9 nm. This specific surface area is significantly higher than that of the undoped sample (38.1 $m^2\ g^{-1}$), while the pore size is more optimized. In contrast, the undoped material has an average pore diameter of 23.8 nm. The enlarged surface area promotes mass transport, and the refined, smaller pore size is believed to favor the stabilization and increased density of active sites, which is consistent with the pore size distribution shown in Fig. S3b.[24,25]

The presence of Pr, Ni, and Fe in the Pr-NiFe LDH was confirmed by XPS spectroscopy, and further analysis of the chemical valence states was conducted to understand the influence of Pr^{3+} incorporation on the charge distribution within NiFe-LDH (Fig. 3a). As shown in Fig. 3b, the Ni 2p XPS spectrum exhibits peaks at 859.1 eV and 877.1 eV, corresponding to Ni^{3+}, along with peaks at 855.9 eV and 874.2 eV assigned to Ni^{2+}. The Ni $2p_{3/2}$ peak in Pr-NiFe LDH exhibits a blue shift of 0.3 eV toward higher binding energy compared to that of NiFe-LDH. This indicates an increase in the proportion of Ni^{3+} in Pr-NiFe LDH, suggesting that Pr^{3+} doping alters the electron density of Ni ions and promotes the formation of higher-valence Ni species, thereby generating more highly active Ni^{3+} sites.[26] As shown in Fig. 3c, the Fe 2p spectra of both Pr-NiFe LDH and NiFe-LDH show two broad peaks at 712.1 eV and 722.3 eV, corresponding to Fe $2p_{3/2}$ and Fe $2p_{1/2}$, respectively, indicating the presence of Fe^{3+}.[27] In Fig. 1d, the peaks located at 934.72 eV and 977.91 eV are attributed to Pr $2p_{3/2}$ and Pr $2p_{1/2}$, respectively, consistent with Pr^{3+} in PrOOH. Notably, after incorporating Pr^{3+} into NiFe-LDH, the two peaks of Fe^{3+} exhibit a red shift of 0.3 eV toward lower binding energy, suggesting a synergistic electronic interaction among Ni, Fe, and Pr ions.

3.1. Electrocatalytic performance

To investigate the effect of Pr^{3+} doping on the OER activity, linear sweep voltammetry (LSV) measurements were conducted in 1 M KOH using a standard three-electrode system, and the results were compared with those of a commercial benchmark RuO_2 catalyst. As shown in Fig. 3a, the current density of Pr-NiFe LDH achieved current densities of 100 mA cm^{-2} with minimum overpotential of 321 mV, which was much lower than that of NiFe-LDH (342 mV), RuO_2 (441 mV) (Fig. 4a). The

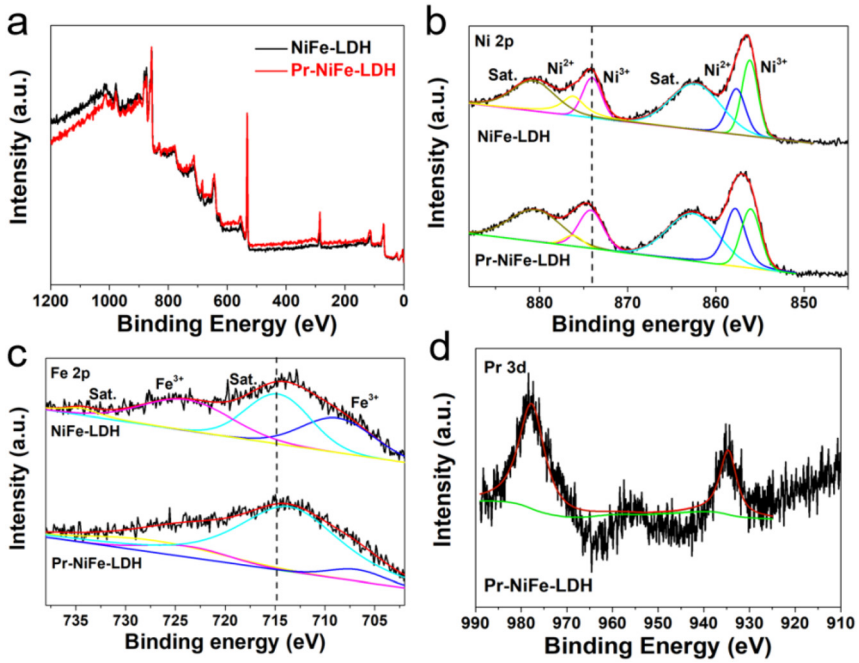

Fig. 3 XPS spectra for (a) full spectrum, (b) Ni 2p, (c) Fe 2p, and (d) Pr 3d of NiFe LDH and Pr-NiFe LDH samples.

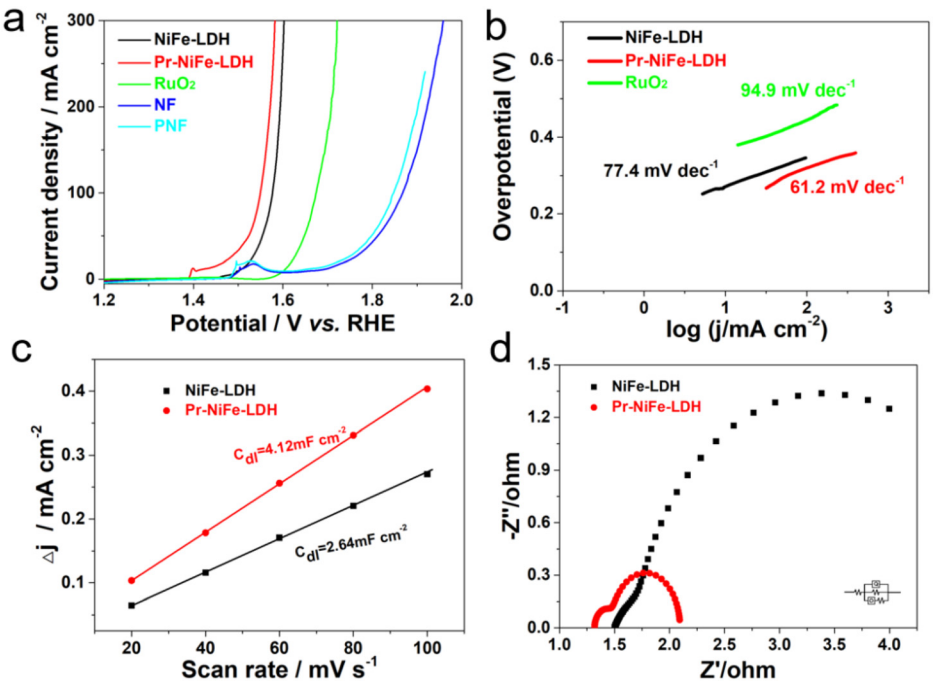

Fig. 4 Electrochemical performance of NiFe LDH and Pr-NiFe LDH electrodes. (a) OER LSV polarization curves of NiFe LDH, Pr-NiFe LDH, RuO_2, NF and PNF. (b) Tafel curves of NiFe LDH, Pr-NiFe LDH and RuO_2. (c) C_{dl} values of NiFe LDH and Pr-NiFe LDH. (d) EIS impedance spectra of NiFe LDH and Pr-NiFe LDH samples.

important point is that the Pr-NiFe LDH catalyst also exhibits significantly superior activity in the OER compared to other catalysts reported so far (Table S1). This result confirms the crucial role of the Pr atoms in enhancing the OER performance of the NiFe catalyst.

Furthermore, the fast OER kinetics were supported by Tafel analysis. As shown in Fig. 4b, the Pr-NiFe LDH catalyst exhibits the smallest Tafel slope of 61.2 mV dec^{-1}, which is lower than those of NiFe LDH (77.4 mV dec^{-1}), RuO_2/NF (94.9 mV dec^{-1}), and other reference catalysts, demonstrating that the incorpor-

ation of Pr significantly enhances the reaction kinetics. Electrochemical impedance spectroscopy (EIS) is used to study the charge transfer ability at the interface of electrocatalysts.[15] The curve radius of Pr-NiFe LDH is the smallest, which indicates that its charge transfer resistance is the lowest (Fig. 4d). This is in good agreement with its lowest Tafel slope, and is also consistent with the above analysis of the thickness of the nanosheets in the SEM image. To evaluate the relative electrochemically active surface areas (ECSAs) of the various catalysts, the double-layer capacitances (C_{dl}) of the electrocatalysts were determined from cyclic voltammetry (CV) measurements within a non-faradaic potential window (Fig. S4). Notably, the C_{dl} value of Pr-NiFe LDH (4.12 mF cm^{-2}) was significantly higher than that of NiFe LDH (2.64 mF cm^{-2}) (Fig. 4c), indicating a larger ECSA and consistent with its enhanced OER activity.[28–30]

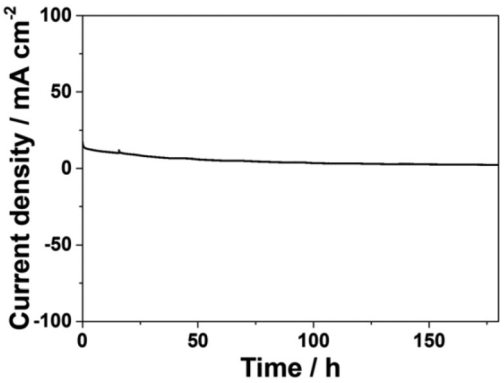

Fig. 5 Chronoamperometric tests.

The electrocatalytic stability and durability of a catalyst are critical metrics for evaluating its OER performance. Furthermore, the electrocatalytic durability of was assessed through a long-term chronoamperometry (i–t) test. Notably, as presented in Fig. 5, the current density remained highly stable with no significant decay over time. These results demonstrate that the as-prepared Pr-NiFe LDH exhibits excellent electrocatalytic durability, which is a prerequisite for its potential application in industrial water splitting. The stability of this integrated electrode was further corroborated by structural analysis of the catalyst used. After electrochemical testing for the oxygen evolution reaction (OER), the Pr-NiFe LDH sample was characterized by XRD, XPS and SEM. As shown in Fig. S5, the XRD pattern of Pr-NiFe LDH after the durability test remains consistent with that of the initial layered hydroxide oxide structure, indicating that the crystal structure of Pr-NiFe LDH remained unchanged before and after testing. Furthermore, the comparison of Pr 3d XPS spectra before and after the test indicates that even after a long period of testing, the signal of the Pr element weakened (Fig. S6). The collapse of the three-dimensional porous structure, as observed by SEM after OER testing, resulted from the bending, fracture, and eventual stacking of the initial sheet-like architecture (Fig. S7). This suggests that the material's mechanical strength was inadequate to withstand the prolonged stresses of electrochemical operation and oxygen bubble evolution. Based on the above results, the Pr-NiFe LDH catalyst is confirmed to be a highly efficient and stable electrocatalyst for the OER.

To gain deeper insights into the critical role of Pr in enhancing the OER performance of NiFe-LDH, we performed theoretical calculations from an energy perspective (Fig. 6a). A comparison of our computational results with relevant literature

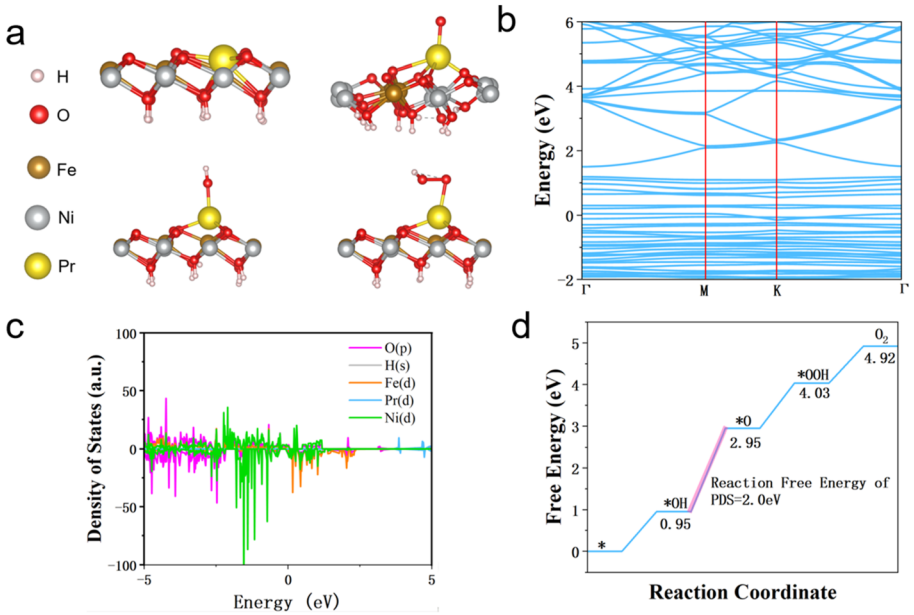

Fig. 6 (a) Mechanism diagram of oxygen evolution process for Pr-NiFe LDH, (b) Pr-NiFe LDH structure band diagram, (c) density of states (DOS) curves of Pr-NiFe LDH, (d) Gibbs free energy diagram for the four steps of OER on Pr-NiFe-LDH.

reveals that the projected density of states (PDOS) of O 2p, Ni 3d, and Fe 3d orbitals in both NiFe-LDH and Pr-NiFe-LDH exhibit similar electronic characteristics (Fig. 6b and c). Moreover, the computed total density of states (DOS) for both systems display metallic behavior, suggesting efficient electron transfer, where the Ni 3d and Fe 3d states dominate the electronic interactions between reaction intermediates and the catalyst surface. In the case of Pr-NiFe-LDH, Pr doping modifies the electronic structure, particularly near the Fermi level. Notably, the d-states of Pr-NiFe-LDH shift closer to the Fermi level, resulting in an upward shift of the d-band center (ε_d), which likely facilitates a more favorable electronic environment for intermediate adsorption.[31,32]

We further investigated the adsorption and transformation of oxygen-containing species (*OH, *O, and *OOH) on Pr-NiFe-LDH. As depicted in Fig. 6a, the sites adjacent to Pr atoms are identified as the primary active centers, owing to the lower energy barrier in the rate-determining step. Specifically, for Pr-NiFe-LDH, the rate-determining step is identified as *OH + $OH^- \rightarrow$ *O + H_2O + e^- (Fig. 6d). In contrast to recent reports on undoped NiFe-LDH, which requires higher energy input for the dehydrogenation of *OH to *O, Pr doping endows Pr-NiFe-LDH with a more favorable energy profile for the rate-determining step (2.0 eV) and reduces the overall reaction energy consumption.[33]

4. Conclusion

In this study, a Pr-doped NiFe layered double hydroxide (LDH) electrocatalyst was synthesized *in situ* on a plasma-activated nickel alloy substrate *via* a one-step hydrothermal method. The as-prepared Pr-NiFe LDH catalyst exhibited outstanding oxygen evolution reaction (OER) activity and excellent stability in 1 M KOH, achieving a current density of 100 mA cm^{-2} at an overpotential as low as 321 mV, which is superior to that of the commercial RuO_2 catalyst (441 mV). The improvement in electrocatalytic performance can be attributed to the faster charge transfer rate and larger electrochemical active surface area after Pr doping. A series of characterization methods and theoretical computational analyses have demonstrated that the lattice distortion and morphology control strategy induced by Pr doping is an effective and feasible approach, which can enhance the oxygen evolution reaction catalytic activity of NiFe-LDH. Therefore, our work paves the way for future studies on highly efficient and stable OER electrocatalysts based on NiFe or even more complex LDH structures.

Author contributions

Jian-Long Lei: investigation. Shui-Sheng Li: formal analysis, data curation. Xi Zhen: methodology, data curation. Lu Shen: formal analysis, data curation. Bin He: writing – review & editing, supervision, project administration.

Conflicts of interest

The authors declare that they have no known competing financial interests or personal relationships that could have appeared to influence the work reported in this paper.

Data availability

All data supporting this study are included in the article and its supplementary information (SI). Supplementary information is available. See DOI: https://doi.org/10.1039/d5dt02658j.

Acknowledgements

This work was financially supported by the the Natural Science Foundations of Zhejiang province (no. LQ24E040002), the School-level Graduate Education.

References

1 G. Y. Zhou, M. X. Pang, J. Li, B. He, Z. J. Li and Y. W. Tang, Interfacial engineering-triggered electronic regulation of Re and CoP hollow multi-shelled structure toward high-activity electrochemical water splitting, *Green Chem.*, 2025, **27**, 13404–13412.
2 C. Ge, Z. J. Li, J. Li, Y. N. Chang, B. He, Y. L. Gu, Y. W. Tang and T. F. Li, Implanting Atomically Dispersed Fe Atoms with Dense Active Sites into Carbon Nanospheres for Efficient Oxygen Reduction Electrocatalysis in Anion Exchange Membrane Fuel Cells, *ACS Sustainable Chem. Eng.*, 2025, **13**, 8999–9008.
3 J. P. Tian, Y. H. Ye, J. Y. Zhou, S. S. Li, B. W. Duan, L. Shen and B. He, Interface electronic coupling in $NiCo_2S_4$ nanorod-amorphous FeOOH nanosheets with enhanced catalytic activity in the oxygen evolution reaction, *New J. Chem.*, 2025, **49**, 6269–6276.
4 W. Z. Jia, Q. Lu, T. Tian, G. X. Pan, R. Tan, B. He and J. Liu, Self-templated fabrication of P-doped $CoMoO_4$-Co_3O_4 hollow nanocages for the efficient oxygen evolution reaction, *Nanoscale*, 2024, **16**, 18076–18085.
5 Y. Liu, J. P. Guo, X. P. Liu, Z. H. Liu, T. Li, S. Wang, C. C. Zhang, K. L. Wang, T. W. Xu, W. J. Kong, Z. J. Chen, J. T. Huang, J. W. Xiao, H. F. Liu, H. Y. Shao and D. L. Wang, Corrosion-Driven Ni_3S_4 Gradient in NiFe-LDH Enables Durable Industrial-Scale Water Electrolysis, *Angew. Chem., Int. Ed.*, 2025, **64**, e202516894.
6 X. Y. Fan, Z. J. Fu, J. Y. Lin, B. He, J. Zhang, E. L. Hu and Z. W. Chen, Modulation of energy barrier of reaction steps over S-doped $Ni(OH)_2$/Cu composites to achieve high-performance urea electrolysis catalysts, *Chem. Eng. J.*, 2024, **490**, 151251.
7 B. He, P. Zhao, G. X. Pan, Q. Lu, H. Q. Li, F. Ye, Y. W. Tang, Q. L. Hao and Z. Su, Interface engineering of NiTe/NiCo-

LDH core-shell structure to enhance oxygen evolution electrocatalysis performance, *J. Alloys Compd.*, 2023, **938**, 168673.

8 Q. Fang, L. J. Wang, D. Yang, L. Xue, W. L. Gu, L. Y. Hu, L. Shi and C. Z. Zhu, Ga-Induced p-d Orbital Hybridization in CoFe LDH for Boosted Oxygen Evolution Electrocatalysis, *ACS Mater. Lett.*, 2024, **6**, 3963–3969.

9 Z. H. Tian, Y. Y. Liu, Z. Y. Chen, Z. Wan, J. Z. Yang, P. L. Zuo, M. X. Ren, P. Hu, F. Teng and H. B. Fan, Ga doping enhances the oxygen evolution reaction performance and stability of NiFe layered double hydroxides, *J. Mater. Chem. A*, 2025, **13**, 16241–16249.

10 T. Sun, B. He, G. X. Pan, Y. H. Guo, K. Y. Wang, W. Z. Jia, Y. C. Guo, P. S. Tang and G. L. Chen, Engineering $NiFe_2O_4$ decorated with IrO_2 on plasma-treated iron foam for enhanced electrocatalytic hydrogen evolution, *J. Colloid Interface Sci.*, 2025, **696**, 137843.

11 G. Y. Zhou, C. Wei, Z. J. Li, B. He, Z. Y. Liu and J. Li, Fe doping and interface engineering-induced dual electronic regulation of $CoSe_2/Co_9S_8$ nanorod arrays for enhanced electrochemical oxygen evolution, *Inorg. Chem. Front.*, 2023, **11**, 164–171.

12 Z. Y. Yang, X. G. Wu, W. Z. Tan, C. Li, S. Shao and X. Y. Meng, Bilayer Heterostructured Ni_3S_2@Ta-NiFe LDH Cross-Linked Nanosheets for Efficient Oxygen Evolution Reaction, *ACS Appl. Mater. Interfaces*, 2025, **17**, 45764–45773.

13 Q. H. Su, P. Y. Wang, Q. C. Liu, R. Sheng, W. H. Cheng, J. Ding, Y. P. Lei and Y. D. Huang, Dual role of sulfur doping in NiCr LDH for water oxidation: Promoting surface reconfiguration and lattice oxygen oxidation, *Appl. Catal., B*, 2024, **351**, 123994.

14 Y. Y. Liao, R. C. He, W. H. Pan, Y. Li, Y. Y. Wang, J. Li and Y. X. Li, Lattice distortion induced Ce-doped NiFe-LDH for efficient oxygen evolution, *Chem. Eng. J.*, 2023, **464**, 142669.

15 G. L. Chen, H. Y. Xiang, Y. C. Guo, J. Huang, W. Chen, Z. Y. Chen, T. T. Li and K. Ostrikov, Yttrium-and nitrogen-doped NiCo phosphide nanosheets for high-efficiency water electrolysis, *Carbon Energy*, 2024, **6**, e522.

16 Y. Zhang, K. K. Xu, B. Zhang, S. D. Guan, X. L. Fu and Z. J. Peng, Pr-doped NiCoP nanowire arrays for efficient hydrogen evolution in both acidic and alkaline media, *J. Alloys Compd.*, 2021, **862**, 158047.

17 H. Abu-Farsakh and A. Qteish, Performance of the modified Becke-Johnson potential employing the pseudopotential plane-wave approach for band structure calculations, *Comput. Mater. Sci.*, 2022, **208**, 111324.

18 S. N. Steinmann and C. Corminboeuf, A generalized-gradient approximation exchange hole model for dispersion coefficients, *J. Chem. Phys.*, 2011, **134**, 044117.

19 A. A. Adllan and A. D. Corso, Ultrasoft pseudopotentials and projector augmented-wave data sets: application to diatomic molecules, *J. Phys.:Condens. Matter*, 2011, **23**, 425501.

20 S. Y. Chen, P. T. Salzbrenner and B. Monserrat, Nonuniform grids for Brillouin zone integration and interpolation, *Phys. Rev. B*, 2022, **106**, 155102.

21 V. Wang, N. Xu, J. C. Liu, G. Tang and W. T. Geng, VASPKIT: A user-friendly interface facilitating high-throughput computing and analysis using VASP code, *Comput. Phys. Commun.*, 2021, **267**, 108033.

22 J. C. Shen, C. H. Luo, S. S. Qiao, Y. Q. Chen, K. X. Fu, J. Q. Xu, J. J. Pei, Y. H. Tang, X. L. Zhang, H. F. Tang, H. Zhang and C. B. Liu, Single-Atom Co-Ultrafine RuO_x Clusters Codecorated TiO_2 Nanosheets Promote Photocatalytic Hydrogen Evolution: Modulating Charge Migration, H^+ Adsorption, and H_2 Desorption of Active Sites, *Adv. Funct. Mater.*, 2024, **34**, 2309056.

23 M. Wang, K. S. Chen, Z. H. Yan, Y. J. Chen, H. T. Liu and X. W. Du, Tailoring the oxygen evolution reaction activity of lanthanide-doped NiFe-LDHs through lanthanide contraction, *Chem. Eng. J.*, 2024, **496**, 154059.

24 S. Z. Asl, F. H. Saboor, D. Seifzadeh, M. Safajou-Jahankhanemlou and M. Asgari, Layered double hydroxide-metal organic framework nanocomposites: A review on their versatile applications in electrocatalysts, supercapacitors, and adsorption, *J. Mol. Struct.*, 2025, **1342**, 142703.

25 N. Ebrahimi, F. Bibak, M. Shakeri and F. Meshkani, The influence of Ce, La, and Y promoters on the catalytic performance of Ni/Cr_2O_3 catalysts for CO_2 methanation, *J. Mol. Struct.*, 2025, **1328**, 141369.

26 S. Q. Lu, A. Wang, A. Y. Jiang and J. L. Zhang, Unveiling the role of bismuth doping in NiFe layered double hydroxide catalysts: Synergistic electronic modulation for superior oxygen evolution activity, *Int. J. Hydrogen Energy*, 2025, **123**, 23–31.

27 X. Y. Wang, Y. X. Tuo, Y. Zhou, D. Wang, S. T. Wang and J. Zhang, Ta-doping triggered electronic structural engineering and strain effect in NiFe LDH for enhanced water oxidation, *Chem. Eng. J.*, 2021, **403**, 126297.

28 W. Z. Jia, Q. Lu, W. J. Zheng, K. Y. Wang, X. H. Liu, S. C. Yang and B. He, V-doped porous CoP nanoarrays grown on carbon cloth with optimized electronic structure for the hydrogen evolution reaction, *Nanoscale Adv.*, 2023, **5**, 4133–4139.

29 M. Zhou, W. Z. Jia, T. Tian, Y. H. Ye, J. Y. Zhou, J. P. Tian, G. X. Pan and B. He, Electronic Structure Engineering of NiCoP Sites via N, Ru Dual Doping for Bifunctional Water Electrolysis, *Inorg. Chem.*, 2024, **63**, 23296–23303.

30 Z. X. Yin, B. Q. Zhang, Q. T. Zhang, Y. Zhou, J. L. Li, Y. P. Wang, L. J. Wan and Z. C. Ma, Graphene quantum dots/$Fe_2(MoO_4)_3$ nanocomposites on Ni form as a efficient (pre)catalyst for OER and HER, *J. Mol. Struct.*, 2025, **1329**, 141402.

31 S. H. Wang, J. Wu, Y. Xu, D. D. Liang, D. Li, D. H. Chen, G. H. Liu and Y. J. Feng, Boosting Efficient Alkaline Hydrogen Evolution Reaction of CoFe-Layered Double Hydroxides Nanosheets via Co-Coordination Mechanism of W-Doping and Oxygen Defect Engineering, *Small*, 2024, **20**, 2311221.

32 Q. Q. Li, F. Z. Huang, S. K. Li, H. Zhang and X. Y. Yu, Oxygen Vacancy Engineering Synergistic with Surface Hydrophilicity Modification of Hollow Ru Doped CoNi-LDH Nanotube Arrays for Boosting Hydrogen Evolution, *Small*, 2022, **18**, 2104323.

33 S. B. Roy, S. Moon, A. Patil, Y. Seo, K. Kang and S. C. Jun, Modulation of charge distribution of $NiCo_2S_4$ by inducing S vacancy and incorporating Ir single atom and cluster catalyst for efficient alkaline water electrolysis, *Mater.Today Energy*, 2025, **54**, 2086.